

Figure 3.22: Simulated extraction of the form factor $(t^2 R_A^{\pi^0})^2$ from Eq. 3.24 compared with theory[14, 15], assuming statistical accuracies obtained as in figure 3.21.

Q^2 . This has been fed into the CLAS⁺⁺ Monte Carlo simulator, to obtain detected events under the assumption of a 2000 hr run with a luminosity of $1 \times 10^{35} \text{ cm}^{-2}\text{s}^{-1}$. The trigger consisted of the coincidence of an electron, proton and the two decay photons. Even with such a restrictive trigger the result yields very favorable counting rate over the entire range of t and Q^2 . Figures 3.21 and 3.22 illustrate some of the results of the simulation. With such favorable statistics we can envision performing L-T separated t distributions over a large range of t .

3.2 Inclusive Nucleon Structure Functions

3.2.1 Overview

Polarized and unpolarized structure functions of the nucleon offer a unique window on the internal quark structure of stable baryons. The study of these structure functions provides insight into the two defining features of QCD — asymptotic freedom at small distances, and confinement and non-perturbative effects at large distance scales. From measurements of structure functions we can infer the fraction of the nucleon momentum and spin carried by quarks, and, via perturbative evolution, by gluons.

After more than three decades of measurements at many accelerator facilities

worldwide, a truly impressive amount of data has been collected, covering several orders of magnitude in both kinematic variables (x , the fraction of the nucleon momentum carried by the struck quark, and the momentum transfer squared, Q^2). However, there are still important regions of the kinematic phase space where data are scarce and have large errors, where significant improvements are possible through experiments at Jefferson Lab with an 11 GeV electron beam.

One of the most interesting open questions is the behavior of the structure functions in the extreme kinematic limit $x \rightarrow 1$, where nearly all of the nucleon momentum is carried by a single quark. In this region the nucleon wave function is dominated by valence quarks, which give the overall charge and baryon number of the nucleon, and effects from the virtual sea of quark-antiquark pairs are suppressed. Understanding of this region requires determining relative size of the contribution from u and d valence quarks, as well as quarks with spin parallel and antiparallel to the nucleon spin. Simple phenomenological models, like the spin-flavor symmetric quark model, predict significantly different behavior from perturbative QCD, or from quark models with hyperfine interactions. Observables such as the neutron to proton structure function ratio, F_2^n/F_2^p , and the polarization asymmetry, A_1 , very sensitive at large x to the details of the quark wave function in the nucleon, and provide excellent laboratories for studying the systematics of spin-flavor symmetry breaking in the nucleon.

In addition to measurements of valence quark structure at large x , the 12 GeV upgrade will allow a detailed study of the phenomenon of quark-hadron duality. Quark-hadron duality refers to the observation, first made by Bloom and Gilman [61], that the structure function in the resonance region, when suitably averaged over an appropriate energy interval, closely follows the scaling structure function measured at higher energies, where the interaction is dominated by single quark scattering. The phenomenon of quark-hadron duality has so far only been shown to exist in the proton structure function F_2^p , but has not yet been studied for neutrons. Duality in other structure functions, such as the longitudinal structure function F_L , or the spin structure functions g_1 and g_2 , is only just beginning to be explored. Understanding the duality between descriptions of a nucleon using either quark or hadronic degrees of freedom in different physical processes and under different kinematical conditions will provide an important key to understanding the consequences of QCD for hadronic structure. Furthermore, both unpolarized and polarized structure functions are not well known at low to moderate Q^2 and x . An improved data sample in this region would allow one to study issues like higher-twist contributions to the structure functions, and improve perturbative QCD analyses by increasing the Q^2 range covered.

The CLAS⁺⁺ detector will allow significant contributions to be made to these studies, particularly in two cases:

- Measurements of the neutron structure function F_2^n in the region of very large x , where we will employ a novel technique (recoil proton detection) to eliminate contamination from nuclear effects, and

- Measurements of polarized structure functions of the proton and deuteron in the region of moderate to high x .

In both cases, the possible luminosity of the experiment is limited by other factors, so that the relatively low luminosity of CLAS will be largely compensated by its very large acceptance.

3.2.2 Neutron structure function at large x

Valence quark distributions

Although a large body of structure function data exists over a wide range of x and Q^2 , the region $x > 0.6$ is not well explored. For $x \geq 0.4$ the contributions from the $q\bar{q}$ sea are negligible, and the structure functions are dominated by the valence quarks.

Knowledge of the valence quark distributions of the nucleon at large x is vital for several reasons. The simplest SU(6) symmetric quark model predicts that the ratio of d to u quark distributions in the proton is $\frac{1}{2}$, however, the breaking of this symmetry in nature leads to a much smaller ratio. Various mechanisms have been invoked to explain why the d distribution is softer than u . For instance, if the interaction between quarks that are spectators to the deep inelastic collision is dominated by one-gluon exchange, the d quark distribution will be suppressed, and the d/u ratio will tend to zero in the limit $x \rightarrow 1$ [62, 63, 64, 65, 66, 67]. This assumption has been built into most global analyses of parton distribution functions [68], and has never been tested independently. On the other hand, if the dominant reaction mechanism involves deep-inelastic scattering from a quark with the same spin orientation as the nucleon, as predicted by perturbative QCD counting rules, then d/u tends to $\approx 1/5$ as $x \rightarrow 1$ [69]. Determining d/u experimentally would lead to important insights into the mechanisms responsible for spin-flavor symmetry breaking. In addition, quark distributions at large x are a crucial input for estimating backgrounds in searches for new physics beyond the Standard Model at high energy colliders [70].

Because of the 4:1 weighting of the squared quark charges between the up and down quarks, data on the proton structure function, F_2^p , provide strong constraints on the u quark distribution at large x ,

$$F_2^p(x) = x \sum_q e_q^2 (q(x) + \bar{q}(x)) \approx x \left(\frac{4}{9} u(x) + \frac{1}{9} d(x) \right). \quad (3.25)$$

The determination of the d quark distributions, on the other hand, requires in addition the measurement of the neutron structure function, F_2^n . In particular, the d/u ratio can be determined (at leading order) from the ratio of neutron to proton structure functions:

$$\frac{F_2^n}{F_2^p} \approx \frac{1 + 4d/u}{4 + d/u}, \quad (3.26)$$

provided $x \geq 0.4$ so that sea quark contributions can be neglected.

Up to now, data on F_2^n have been extracted primarily from inclusive scattering off deuterium. Unfortunately, theoretical uncertainties in the treatment of nuclear corrections have led to ambiguities in the extracted F_2^n at large x . In particular, inclusion of Fermi motion and nucleon off-shell corrections in the deuteron can lead to values for F_2^n/F_2^p that differ by 50% already at $x = 0.75$ [71, 72] compared with values extracted assuming the presence of Fermi motion corrections only. The differences are even more dramatic if one extracts F_2^n on the basis of the nuclear density model [73]. The tagged structure function method for measuring F_2^n proposed here on the other hand virtually eliminates the uncertainties from nuclear models.

Resonance region

In addition to the deep-inelastic region, it is also important to map out the neutron resonance region, where at present there are essentially no data. Resonance transition and elastic form factors provide fundamental information on the structure of the neutron, and therefore are very interesting in their own right.

Measurements [74, 75] at Jefferson Lab of the unpolarized structure functions on hydrogen in the resonance region have previously been used to verify Bloom-Gilman duality [61, 76]. These have inspired considerable interest in quark-hadron duality [77], and neutron data will add more valuable information. Within a simple harmonic oscillator quark model, Close and Isgur [78] found that the neutron structure functions should exhibit systematic deviations from local duality, and that duality should occur at higher W for the neutron than for the proton. Understanding duality could prove to be crucial for mapping the transition from hadronic to quark-gluon degrees of freedom, and the measurements proposed here would allow one to identify the basic principles which underly this transition. Furthermore, if the systematics of Bloom-Gilman duality are understood quantitatively, duality could provide a powerful tool for accessing the large x region.

Although precision electron-proton scattering experiments have been performed in a straightforward manner with hydrogen targets, it has been necessary to infer experimental information on the structure of the neutron from nuclear (typically deuteron) data. The procedure of unfolding neutron data from inclusive nuclear cross sections, via the subtraction of Fermi motion effects and contributions from various nuclear constituents, leads to ambiguities dependent on the models and reaction mechanisms employed. This is particularly true for measurements in the elastic and resonance regions at high x and moderate Q^2 .

To illustrate this, consider the inclusive resonance electroproduction cross section spectra shown in Fig. 3.23. These data were obtained at Jefferson Lab at $Q^2 = 1.5$ (GeV/c)² for hydrogen and deuterium targets at matched kinematics. Although the three prominent resonance enhancements are obvious in the hydrogen data, only a hint of the first (the $\Delta(1232)$) is identifiable in the deuterium data. At

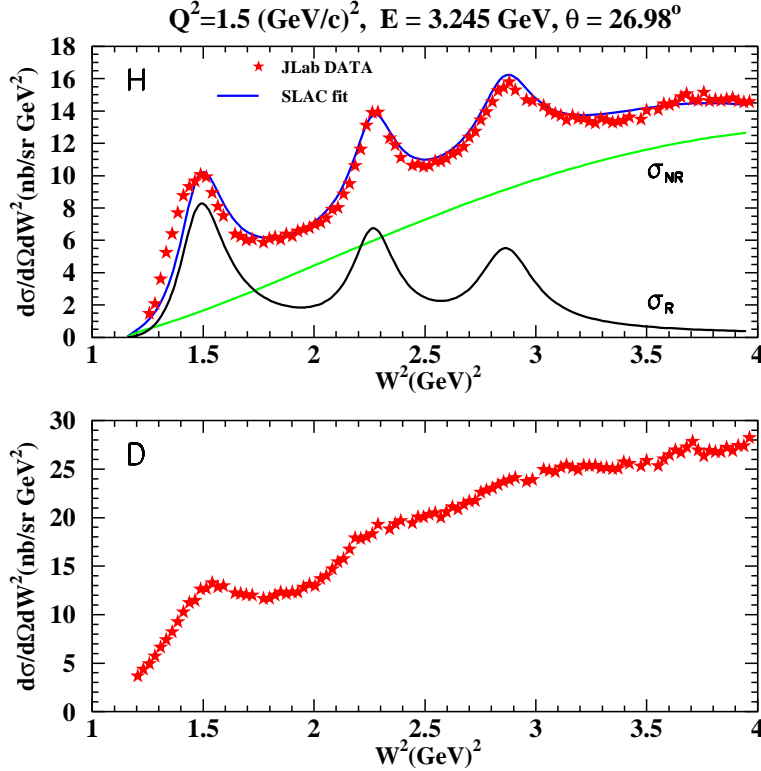


Figure 3.23: Inclusive resonance electroproduction cross sections from Jefferson Lab at $Q^2 = 1.5 \text{ (GeV/c)}^2$ [79]. Cross sections are shown as a function of invariant mass squared for hydrogen (top) deuterium (bottom) targets at matched kinematics. The hydrogen spectrum is plotted with global resonant and non-resonant fits.

$Q^2 > 2 \text{ (GeV/c)}^2$, no discernable structure remains in the deuterium data. Neutron extraction from such data requires careful modeling of the resonant and non-resonant components for the neutron (as was done with the hydrogen data). Calculations must account for the nuclear effects of binding, Fermi motion, and nucleon off-shellness, and the model-dependence introduced by each of these steps leads to a substantial uncertainty in the neutron resonance structure functions. For this reason very little neutron resonance transition form factor data exist.

Tagged structure functions

The measurement of the tagged structure functions in semi-inclusive scattering from the deuteron with a slow recoil proton detected in the backward hemisphere, $e + D \rightarrow e + p + X$, will allow the structure function of the free neutron to be extracted with minimal ambiguities associated with the nuclear model dependence [80, 81, 82]. Within the nuclear impulse approximation, in which the deep inelastic scattering takes place incoherently from individual nucleons, the differential semi-inclusive cross

section can be written as a product of the deuteron spectral function, \mathcal{S} , and an effective (bound) neutron structure function, $F_2^{n(eff)}$ [82]:

$$\frac{d\sigma}{dx dW^2 d\alpha_{sp} d^2 p_T} \approx \frac{2\alpha_{em}^2(1-\nu/E)}{Q^4} \alpha_{sp} \mathcal{S}(\alpha_{sp}, p_T) F_2^{n(eff)}(W^2, Q^2, p^2). \quad (3.27)$$

Here $W^2 = (p_d + q - p_s)^2$ is the invariant mass squared of the unobserved hadronic final state, with p_s the momentum of the spectator proton, p_d the momentum of the initial state deuteron, and $p = p_d - p_s$ the momentum of the struck neutron. The variable $\alpha_{sp} = (E_s - p_s^z)/M$ is the light-cone momentum fraction carried by the spectator proton and p_T its momentum component perpendicular to the direction of \vec{q} , with $E_s = \sqrt{M^2 + \vec{p}_s^2}$ the spectator proton energy and M its mass. The degree to which the struck neutron is off-shell is given by

$$M^2 - p^2 \approx 2\vec{p}_s^2 + 2M\epsilon, \quad (3.28)$$

where ϵ is the deuteron binding energy. In the limit $p^2 \rightarrow M^2$, the effective neutron structure function $F_2^{n(eff)}(W^2, Q^2, p^2) \rightarrow F_2^n(W^2, Q^2, M^2) \equiv F_2^n(x, Q^2)$, the free neutron structure function. The p^2 dependence of $F_2^{n(eff)}$ depends strongly on the theoretical assumptions made about the off-shell behavior of the photon—bound-nucleon scattering amplitude. The ratio $R_n \equiv F_2^{n(eff)}(W^2, Q^2, p^2)/F_2^n(W^2, Q^2)$ of the bound to free neutron structure functions in the relativistic spectator model of Ref. [83] is shown in Fig. 3.24 for several values of x , as a function of the momentum of the spectator, $|\vec{p}_s| = |\vec{p}|$. Although the effect at low $|\vec{p}_s|$ is small, the deviation from unity increases sharply with increasing momentum, especially at larger values of x where the EMC effect is more pronounced. A similar behavior is observed in the non-relativistic model of Ref. [84], where the assumption of weak binding in the deuteron allows one to calculate the off-shell dependence up to order p^2/M^2 [84].

On the other hand, the color screening model for the suppression of point-like configurations (PLC) in bound nucleons [73], which attributes most or all of the EMC effect to a medium modification of the internal structure of the bound nucleon, predicts somewhat larger (by a factor of 2 or 3 [82]) deviations from unity than those in Fig. 3.24. It is important, therefore, that the tagged structure functions be measured for kinematics where the difference $p^2 - M^2$ is as small as possible, to minimize theoretical uncertainties associated with extrapolation to the nucleon pole. Since the deviation of the bound to free structure function ratio from the free limit is proportional to $2\vec{p}_s^2 + 2M\epsilon$, sampling the data as a function of \vec{p}_s^2 should provide guidance for a smooth extrapolation to the pole. In practice, considering a momentum interval of 70–200 MeV/c would allow the dependence on p^2 to be constrained. Existing 6 GeV data from experiment E94-102 (E6) will help to study the high-virtuality behavior of the bound structure function.

Moreover, extrapolation from the minimum $|\vec{p}| \approx 70$ MeV/c, where the bound neutron is only around 10 MeV away from its mass-shell, should be relatively free

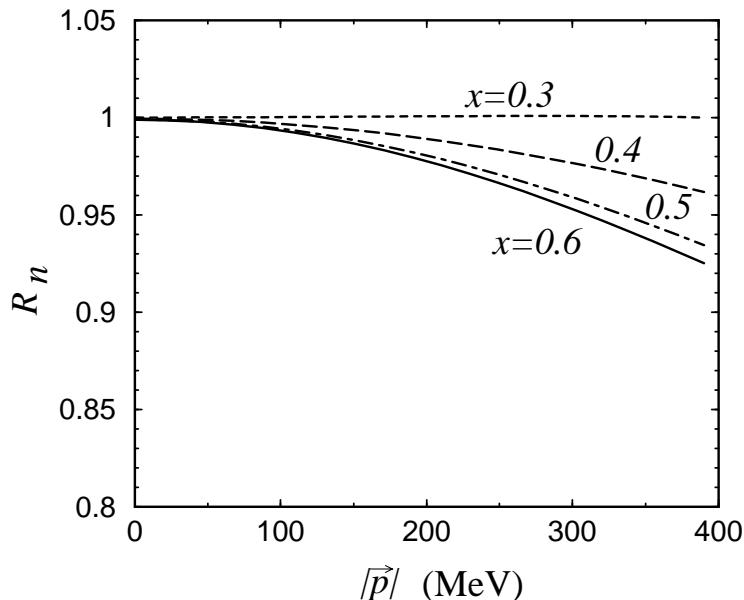


Figure 3.24: The ratio $R_n \equiv F_2^{n(eff)}(W^2, Q^2, p^2)/F_2^n(W^2, Q^2)$ of the bound to free neutron structure functions as a function of the spectator proton momentum in the model of Ref. [83].

of ambiguities. This is also supported by recent ${}^4\text{He}(\vec{e}, e'\vec{p})$ polarization transfer experiments at Mainz and Jefferson Lab which indicate that the magnitude of the off-shell deformation is rather small [85]. These experiments measured the ratio of transverse to longitudinal polarization of the ejected protons, which is related to the medium modification of the electric to magnetic elastic form factor ratio. Using model independent relations derived from quark-hadron duality, one can relate the small, but non-zero medium modification observed in the form factors to a modification at large x of the deep inelastic structure function of the bound nucleon [86], which suggests an effect of $\leq 3\%$ for $x \leq 0.8$. The typical momentum of the knocked out protons in the experiments was ~ 50 MeV, although the results of the analysis were found not to depend strongly on the proton momentum [86]. These considerations lead us to expect that the extrapolation of the bound neutron structure function to the nucleon pole should introduce minimal uncertainty into the extracted structure function of the free neutron.

In addition to determining the free neutron structure function, tagged structure function measurements on the deuteron could allow one to discriminate between different hypotheses on the origin of the nuclear EMC effect [82]. In particular, one may be able to distinguish between models in which the effect arises entirely from hadronic degrees of freedom — nucleons and pions, and models in which the effect is attributed to the explicit deformation of the wave function of the bound nucleon itself. By comparing ratios of semi-inclusive cross sections at different values of x ,

which further reduces the dependence on the deuteron spectral function [73], one can discriminate between models such as the PLC suppression and Q^2 rescaling models, which predict a fast drop with α_{sp} , and nuclear binding models, in which the α_{sp} dependence is quite weak [82]. Furthermore, these studies would enable one to test the validity of factorization in nuclear DIS, and determine the boundaries of the traditional convolution approach to describing nuclear structure functions.

Final state interactions

Another possible source of uncertainty lies in the rescattering, or final state interactions (FSI), of the spectator proton and the deep-inelastic remnants, X , of the scattered neutron. Extraction of the free neutron structure function is most reliable in the kinematic region where the FSI effects are small, and where different nuclear models for the deuteron spectral function, \mathcal{S} , lead to similar results. The choice of backward angles is designed to minimize these effects. Production of backward protons also suppresses contributions from direct processes, where a nucleon is produced at the γ^*N interaction vertex.

The magnitude of FSI effects has been estimated in Ref. [82] within the framework of the distorted wave impulse approximation (DWIA) [87]. Although a direct calculation of the FSI contribution to the cross section requires knowledge of the full dynamics of the spectator proton–neutron remnant system, which is currently unavailable, one can estimate the uncertainty introduced through neglect of FSI by comparing with the calculation of FSI effects in the high-energy $d(e, e'p)n$ break-up reaction [87]. The effective p – X interaction cross section, σ_{eff} , can be approximated [88] by that extracted from soft neutron production in the high-energy DIS of muons from heavy nuclei [89]. The effect of the FSI is to modify the spectral function $\mathcal{S} \rightarrow \mathcal{S}^{DWIA}$ [87], where

$$\mathcal{S}^{DWIA}(\alpha_{sp}, p_T \approx 0) \sim \mathcal{S}(\alpha_{sp}, p_T \approx 0) \left[1 - \frac{\sigma_{eff}(Q^2, x)}{8\pi \langle r_{pn}^2 \rangle} \frac{|\psi_D(\alpha_{sp}, \langle p_T \rangle)\psi_D(\alpha_{sp}, 0)|}{S(\alpha_{sp}, p_T \approx 0)/\sqrt{E_s E_s(\langle p_T^2 \rangle)}} \right]. \quad (3.29)$$

Here $\langle r_{pn}^2 \rangle$ is the average separation of the nucleons within the deuteron, E_s is the spectator nucleon energy, and $E_s(\langle p_T^2 \rangle) = \sqrt{M^2 + p_z^s{}^2 + \langle p_T^2 \rangle}$ is the energy evaluated at the average transverse momentum $\langle p_T^2 \rangle^{1/2} \sim 200\text{--}300$ MeV/c transferred for the hadronic soft interactions, with effective cross section σ_{eff} . The steep momentum dependence of the deuteron wave function, $|\psi_D(\alpha_{sp}, \langle p_T \rangle)| \ll |\psi_D(\alpha_{sp}, p_T \approx 0)|$, ensures that FSI effects are suppressed in the extreme backward kinematics.

The effects of FSI are illustrated in Fig.3.25, which shows the ratio of the light-cone spectral function including FSI effects within the DWIA to that without [82]. At extreme backward kinematics ($p_T \approx 0$) one sees that FSI effects contribute less than $\sim 5\%$ to the overall uncertainty of the $d(e, e'n)X$ cross section for $\alpha_{sp} \leq 1.5$.

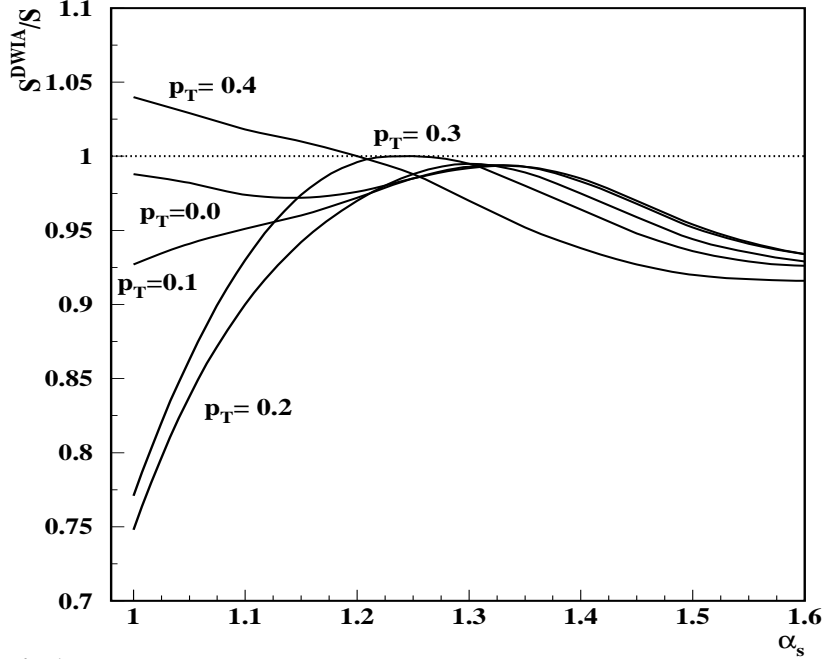


Fig.1

Figure 3.25: Spectral function calculated with and without FSI effects within the DWIA [82]. The curves correspond to different values of the spectator proton transverse momentum (in GeV/c).

This number can be considered as an upper limit on the uncertainties due to FSI. At larger p_T (≥ 0.3 GeV/c) and small α_{sp} (≈ 1) the double scattering contribution (which is not present for the extreme backward case, see Eq. (3.29)) plays a more important role in FSI [87].

At very large x values ($x \geq 0.7$) the factorization approximation itself breaks down [83], and higher order corrections to Eq. (3.27) must be included if one wants accuracy to within a few %. To avoid theoretical ambiguities one should therefore restrict the analysis to spectator momenta below $\approx 150 - 200$ MeV/c.

Of course, in order to identify any residual nuclear effects, it would be ideal to repeat this experiment by detecting spectator neutrons. Comparing the bound proton structure function with the free proton structure function would then allow one to correct the bound neutron structure function for any remaining nuclear effects.

Expected results

We have simulated the expected results from a 40 day (100% efficient) run at 11 GeV in CLAS⁺⁺ with the recoil detector described in Section 5.3. A minimum momentum of 70 MeV/c was assumed for proper detection of a proton moving perpendicular to the detector axis, and accordingly more (due to energy loss) for protons at different angles. A simple model is used of the acceptance of both CLAS⁺⁺ for the scattered electrons and of the recoil detector for protons. To select events where the neutron is close to on-shell, the recoil momentum is required to be less than 180 MeV/c. The spectator proton is also required to make an angle of at least 110 degrees with the

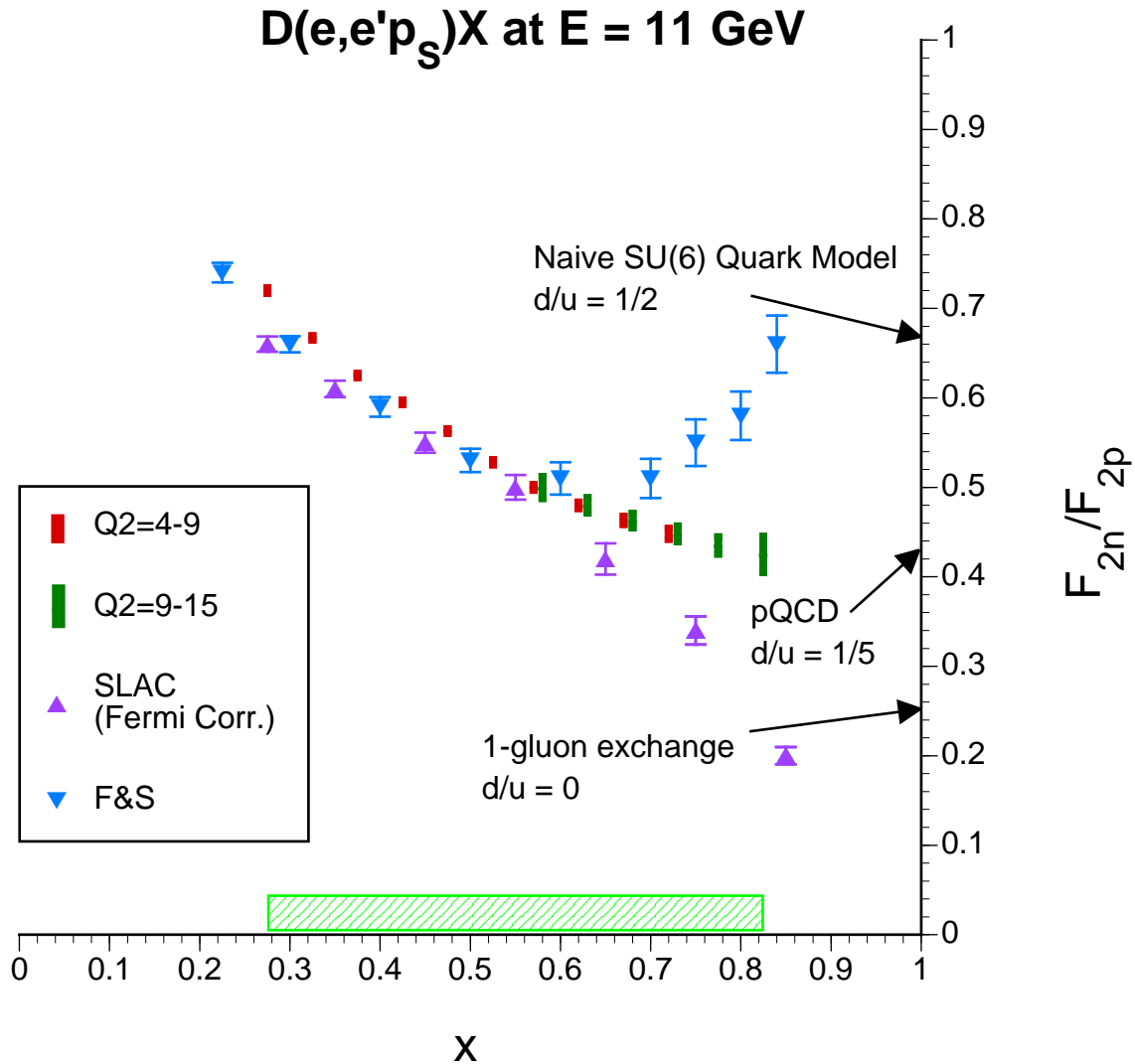


Figure 3.26: Ratio of the neutron and proton structure functions, F_2^n and F_2^p , as a function of x . The red and green vertical bars indicate the expected statistical precision of the proposed experiment for two different bins in Q^2 , based on a 40 day run with full reconstruction of the kinematics via detection of a backward moving spectator proton. The triangles indicate existing (deuterium and proton) data from SLAC (with systematic and statistical error bars combined), analyzed in two different ways, as explained in the text.

direction of the momentum transfer vector, \vec{q} .

Under these conditions, a total of 1.7 M coincident events is expected, and 700 k events with recoil momentum below 100 MeV/c. The average spectator light-cone fraction for these kinematics will be $\alpha_{sp} = 1.1$. A range in W from the elastic peak to about $W = 4$ GeV will be covered. Restricting the kinematics to $W > 1.8$ GeV (where resonant final states have little influence), data for x between 0.1 and 0.85 will be collected, with sufficient statistics to bin in several Q^2 bins from 1 to 15 (GeV/c)² and to study the dependence on the recoil momentum.

As an example, we show in Fig. 3.26 the statistical precision which can be achieved for the ratio F_2^n/F_2^p at high x . The estimated systematic errors, which include experimental and theoretical uncertainties due to FSI effects and possible medium modifications of the nucleon structure function, are indicated by the band along the abscissa. The arrows along the ordinate indicate predictions of different models for the $x \rightarrow 1$ limit, as discussed in Section , which cannot be excluded by present-day data due to the uncertainty in the nuclear effects [72]. The data shown, indicated by triangles, are extracted from proton and deuteron cross sections measured at SLAC (with systematic and statistical error bars combined), analyzed according to different prescriptions for subtracting the nuclear corrections. In one case (upward pointing triangles), the deuterium data were corrected only for Fermi motion [71], while in the other case (downward pointing triangles) a parameterization of the EMC effect based on effective inter-nucleon distances extrapolated to the deuteron [73] was used. Clearly, while the current data cannot discriminate between any of the theoretical predictions, the F_2^n/F_2^p data obtained using the new method will allow us (for the first time) to differentiate unambiguously between different expectations for this ratio.

3.2.3 Spin Structure Functions

Measurement goals

While the behavior of the spin-averaged quark distributions at large x still awaits definitive resolution, our lack of understanding of the spin-dependent distributions at large x is even more striking. For instance, there are a number of qualitatively different predictions for the polarization asymmetry, A_1 , which (in lowest order in perturbative QCD) is given by the ratio of the spin-dependent to spin-averaged quark distributions,

$$A_1(x) = \frac{\sum_q e_q^2 \Delta q(x)}{\sum_q e_q^2 q(x)}, \quad (3.30)$$

where e_q is the quark charge. Arguments based on perturbative one-gluon exchange suggest that this should approach unity as $x \rightarrow 1$ for proton, neutron and (neglecting nuclear correction) deuteron targets [69]. In contrast, nonperturbative models such as those based on SU(6) spin-flavor symmetry predict that $A_{1p} = 5/9$, $A_{1n} = 0$ and

$A_{1d} = 1/3$ [63, 64, 65]. Presently, the world data set is unable to determine the veracity of these predictions.

Although SU(6) symmetry imposes strict relations between the individual quark distributions, such as $\Delta u = -4\Delta d$, in nature this symmetry is strongly broken. Nonperturbative models which break SU(6) symmetry typically involve a hyperfine interaction, derived for instance from one-gluon exchange or pion exchange, which has the effect of suppressing the d quark distribution relative to the u [63, 64, 66, 67]. If the u quark is dominant as $x \rightarrow 1$, the asymmetries A_{1p} , A_{1n} and (in the absence of nuclear effects) A_{1d} will all tend to unity, and distinguishing between the predictions derived from perturbative QCD will require very accurate data at $x \sim 0.6 - 0.8$. On the other hand, the one-gluon exchange model predicts qualitatively different behavior for the ratios of individual distributions $\Delta q/q$, especially for the d quark. While the asymptotic $x \rightarrow 1$ limit in perturbative QCD is $\Delta d/d \rightarrow 1$, one-gluon exchange predicts $\Delta d/d \rightarrow -1/3$ as $x \rightarrow 1$, so that even the sign of the predictions differs.

The ratio $\Delta d/d$ can be extracted from semi-inclusive measurements of pions in the current fragmentation region (see section on semi-inclusive processes). A program of inclusive and semi-inclusive double spin asymmetry measurements using an energy upgraded CEBAF, in conjunction with polarized proton and deuteron targets, can substantially improve our ability to distinguish between the various descriptions of the nucleon.

The large acceptance coverage of CLAS combined with the high luminosity available at an energy upgraded CEBAF will allow access to a large range of x and Q^2 . This will enable precise measurements to be made of moments, or integrals, of the g_1 structure function, and thereby tightly constrain theoretical descriptions of the transition from low to high Q^2 [90, 91, 92]. Understanding this transition is vital for a number of reasons. Through the phenomenon of quark-hadron duality, as discussed in the previous section, one can relate the physics of nucleon resonances, which are described by coherent scattering from constituent quarks at low energy, to the dynamics of single quark scattering which governs the scaling structure function at high energy.

While the phenomenon of quark-hadron duality has been observed in the spin-independent F_2 structure function [74, 61], it has not yet been established for spin-dependent structure functions. Because the g_1 structure function is given by a difference of cross sections, which need not be positive, the workings of duality will necessarily be more intricate for g_1 than for the spin-averaged F_2 structure function. Unlike the unpolarized structure functions, spin 1/2 and 3/2 resonances contribute with opposite signs. For fixed Q^2 values less than 1 (GeV/c)², the $\Delta(1232)$ resonance pulls the g_1 structure function below zero, in contrast to the positive value observed in DIS. This is also related to the physics which drives the dramatic variation of the integral of the g_1 structure function from its large and negative value at $Q^2 = 0$ (where it is related to the Gerasimov-Drell-Hearn sum rule) to a positive value at

large Q^2 (where it is related to deep inelastic sum rules such as the Bjorken sum rule) [90]. Duality may be realized for polarized structure functions if one averages over a complete set of resonances [78]. To achieve a more complete understanding of duality it is necessary to determine the conditions under which duality occurs in both polarized and unpolarized structure functions.

In the context of QCD, one can relate quark-hadron duality to an operator product expansion of moments of structure functions [76]. According to the twist expansion, moments can be expressed in terms of a power series in $1/Q^2$, where the coefficients of each of the terms in the series are related to matrix elements of quark and gluon operators of a certain twist (which is equal to the difference between the mass dimension and spin of an operator) [91, 92]. The leading, Q^2 -independent term is related to matrix elements of quark bilinear operators, and gives rise to the scaling of the structure function. The higher order terms involve matrix elements of mixed quark-gluon field operators, and characterize the effect of background color electric and magnetic fields on quarks [93]. Because of the $1/Q^2$ suppression, extraction of the higher twist matrix elements, which reflect the role played by quark-gluon correlations in the nucleon, requires structure function moments over a large range of Q^2 , from ~ 0.5 (GeV/c) 2 to several (GeV/c) 2 . Measurement of moments of the g_1^p and g_1^d structure functions using CLAS $^{++}$ would therefore significantly improve our understanding of the workings of QCD at low energy.

Future installation of a transversely polarized target will, in addition, allow measurements of the g_2 structure function, which is the cleanest example of a higher twist effect in the nucleon. Although the g_2 structure function does not have a simple parton model interpretation, the x^2 -weighted integral of g_2 is directly related to the color electric and magnetic polarizabilities of the nucleon [93]. In particular, the x^2 moment of the combination $2g_1 + 3g_2$ gives the pure twist-3 matrix element, d_2 , which reflects the strength of nonperturbative quark-gluon correlations in the nucleon. Furthermore, the large kinematic coverage of CLAS $^{++}$ ($0.1 \leq x \leq 0.85$) will allow hitherto unverified sum rules involving g_2 [94, 95] to be tested accurately. A program of transversely polarized structure function measurements would thus open up a whole additional avenue for exploring the transition between asymptotic freedom and confinement physics.

Experimental parameters

For the measurements of spin structure functions in CLAS at 11 GeV, we anticipate that a dedicated polarized target similar to the existing EG1 target will be built (see corresponding sections of the technical section of the CDR). It will contain dynamically polarized solid ammonia ($^{15}\text{NH}_3$ and $^{15}\text{ND}_3$) at about 1K temperature in a 5 Tesla field.

For longitudinal asymmetry measurements, the magnet axis will point along the beam direction. In this case, the acceptance of the target will fully match the accep-

tance of the upgraded CLAS. For transverse asymmetries, the holding field of 5 Tesla will point sideways. Assuming optimized coil openings, we expect a maximum acceptance of ± 20 degrees horizontally and ± 35 degrees vertically. The Møller electrons will be ejected sideways, where they can be contained in massive shielding plates. The electron beam will go through a chicane of one upbending and two downbending magnets, so that it will enter the polarized target pointing down and then be bent into the normal beam line to the electron dump.

For the following rate estimates, we assume 40 ideal running days (corresponding to 3 calendar months) for each target configuration and both NH_3 and ND_3 , and a beam polarization of 70% on average. We expect average target polarizations of 80% for NH_3 and 40% for ND_3 targets, in agreement with recent experience at JLab and SLAC. The overall dilution factor (ratio of events from polarized nucleons to all events) for these targets is about 0.13 for NH_3 and 0.23 for ND_3 , due to the presence of ^{15}N in the ammonia and liquid helium coolant as well as entrance and exit foils. We will run with about 30 nA beam current, rastered over the surface of the targets of length 1.5 cm, yielding an overall luminosity of about $10^{35} \text{ cm}^{-2}\text{s}^{-1}$. Note that this luminosity is only a factor 5 lower than the highest luminosity that can typically be achieved for solid state polarized targets. This makes CLAS a superior choice for measurements with these targets, since the large solid angle (about one steradian) compensates for the limited luminosity, and all kinematic points can be measured simultaneously.

Expected results

The precision that can be achieved for the asymmetry A_{1p} is shown in Fig. 3.27. These data will clearly distinguish between the $\text{SU}(6)$ symmetric quark model prediction of $5/9$ and the pQCD prediction of unity for the limit $x \rightarrow 1$, and dramatically improve our knowledge of the proton's spin structure at high x . The difference between these predictions is even more striking for the deuteron, where we will also be able to significantly improve on existing data, as shown in Fig. 3.28. The high precision data on both the proton and deuteron that will be accumulated for several bins in Q^2 will constrain the logarithmic and $1/Q^2$ scaling violations of the spin structure functions g_1 , and determine their higher moments, as well as allow duality for spin structure functions to be studied in detail.

Finally, the structure function g_{2p} will be determined from data with transverse target polarization. We will again improve significantly on the existing SLAC data, with smaller error bars and finer binning in x and Q^2 . This will allow the evolution of this structure function to be studied and the twist-3 matrix element d_2 to be extracted with three times smaller statistical error than at present.

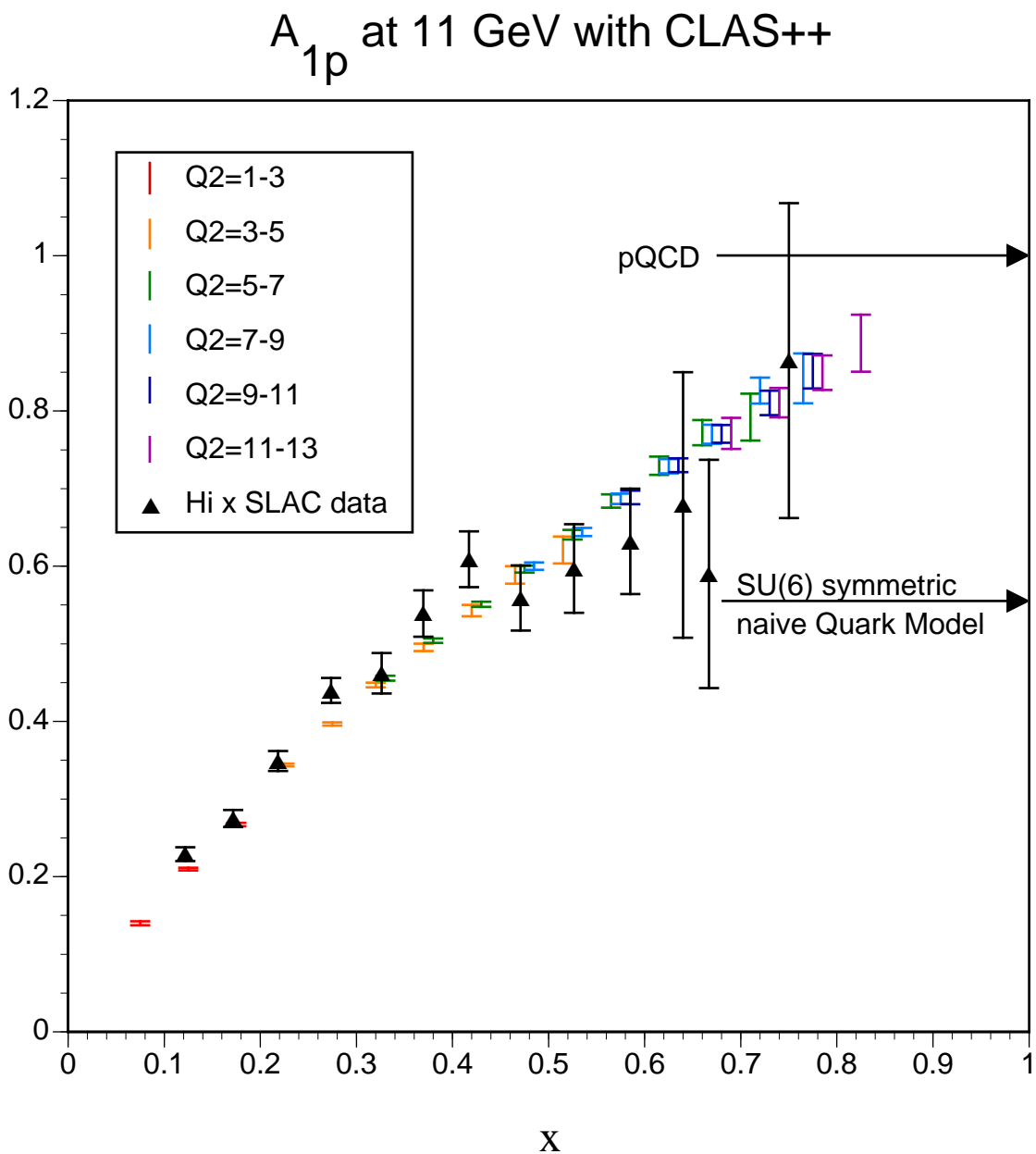


Figure 3.27: Expected data with statistical errors for A_{1p} from 40 days of running with 11 GeV beam. Several bins in Q^2 are indicated by slightly offset error bars. Existing SLAC data (from E130, E143 and E155) are shown as well. The predicted approach to the limit $x = 1$ for two different models is indicated.

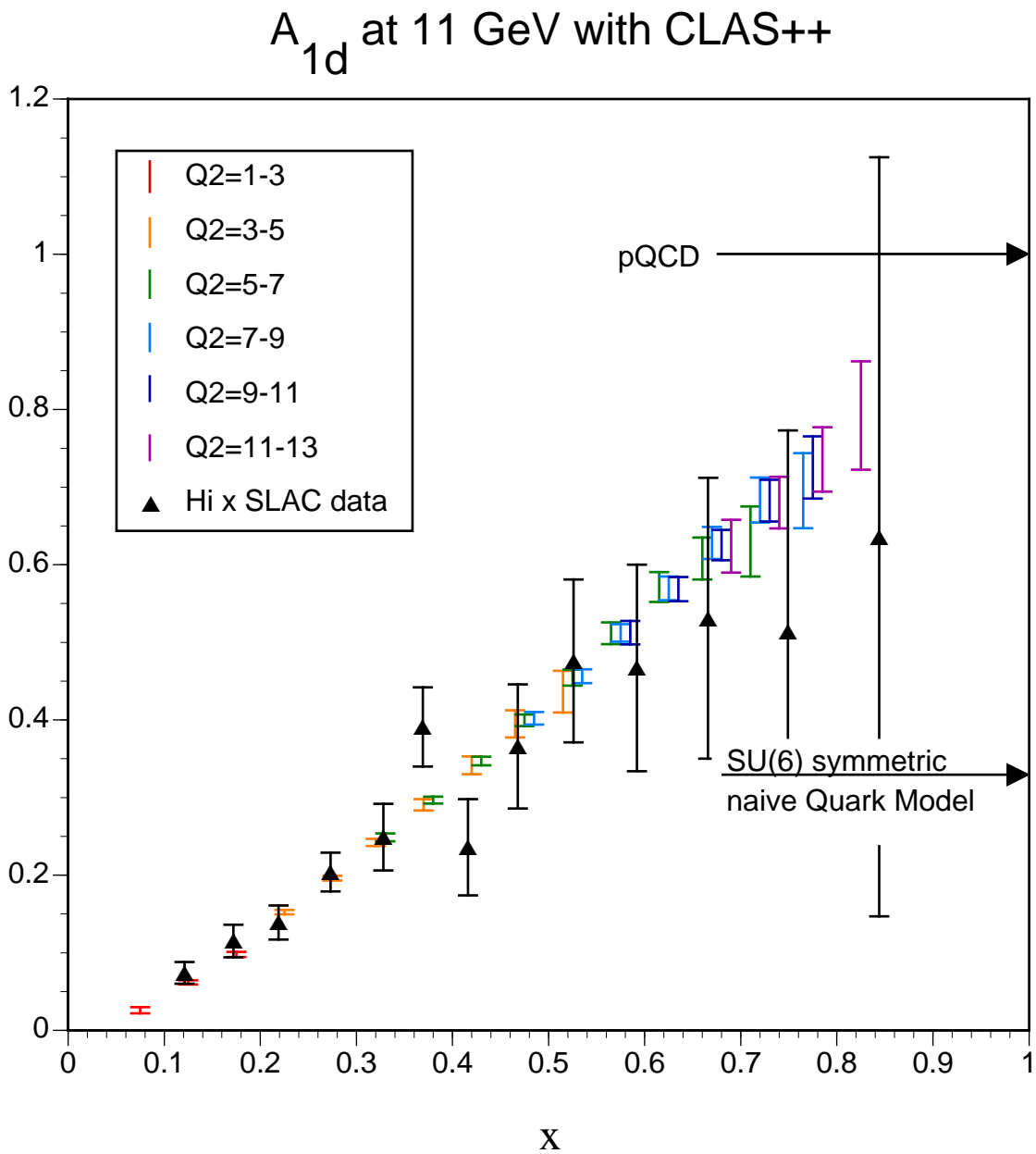


Figure 3.28: Expected data with statistical error bars for A_{1d} for the deuteron from 40 days of running with 11 GeV beam. All symbols are as in Fig. 3.27.

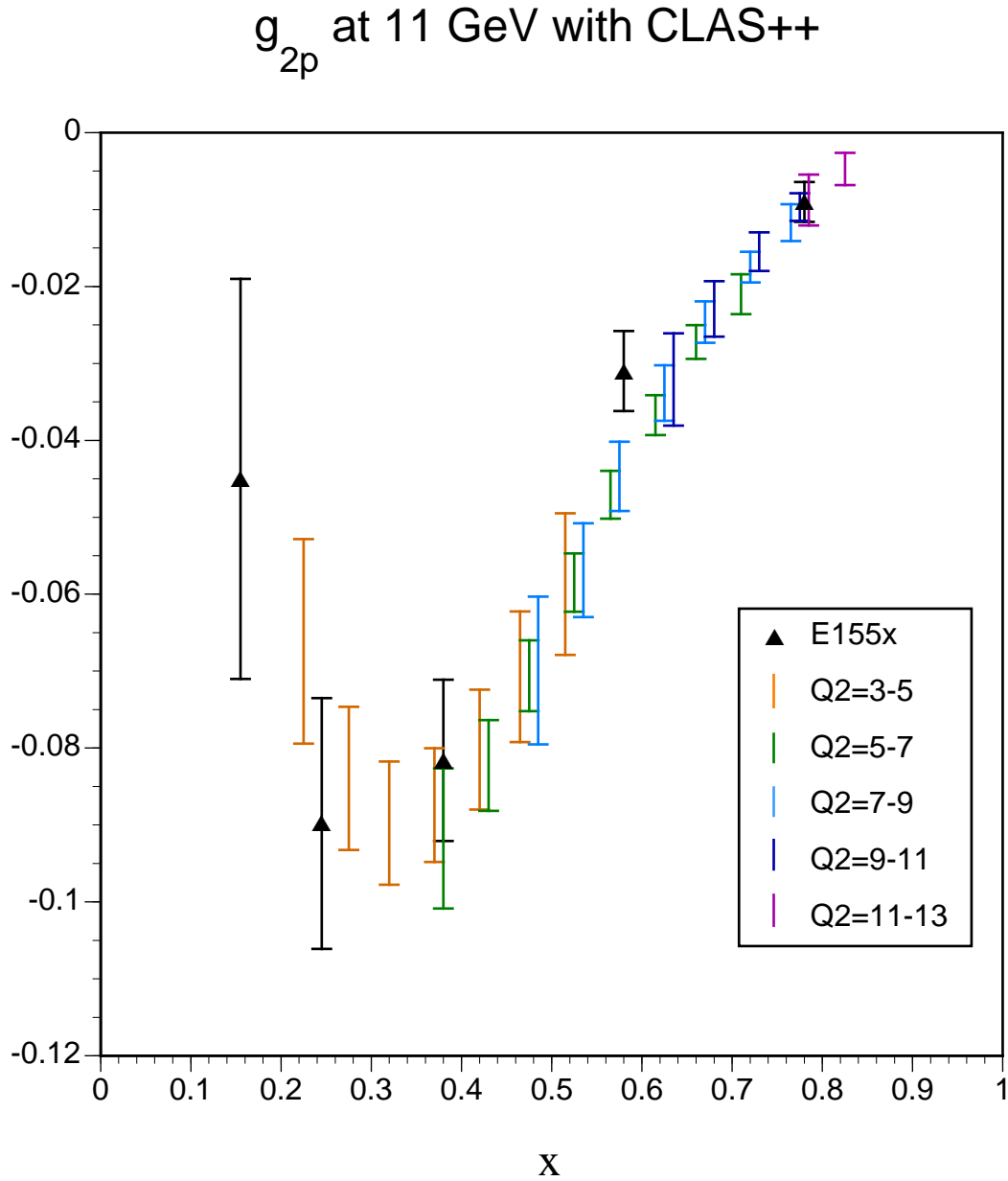


Figure 3.29: Expected statistical error bars on the structure function g_{2p} for the proton from 40 days of running with 11 GeV beam with transverse target polarization.